REVIEW

Fiber Bragg grating pressure sensors: a review

Siyi Xu,[a,b] **Xiaozhi Li**,[a,b] **Tanyu Wang**,[a,b] **Xiujuan Wang**,[a,c,d,*] **and Hao Liu**[a,b,*]

[a]Tiangong University, School of Textile Science and Engineering, Tianjin, China
[b]Tiangong University, Institute of Smart Wearable Electronic Textiles, Tianjin, China
[c]Aerospace Life-Supports Industries Ltd., Xiangyang, China
[d]Aviation Key Laboratory of Science and Technology on Life-Support Technology, Xiangyang, China

Abstract. Fiber Bragg grating (FBG) pressure sensors have the potential to replace conventional voltage sensors due to their compact size, resistance to electromagnetic interference, excellent safety, distributed sensing, and numerous other intrinsic benefits. It is frequently employed in the domains of civil engineering, aerospace, and medicine. Our work examines two types of sensitized FBG pressure sensors, namely FBG pressure sensors with innately improved sensitivity and FBG pressure sensors with extrinsically increased sensitivity. Our work examines microstructured fiber Bragg grating pressure sensors and polymer fiber Bragg grating pressure sensors for FBG pressure sensors with innately heightened sensitivity. Our research examines metal-mechanical FBG pressure sensors and polymer-mechanical FBG pressure sensors for extrinsically sensitized FBG pressure sensors. This report also summarizes the benefits and drawbacks of various FBG pressure sensors and temperature compensation techniques. Finally, the future of FBG pressure sensors is examined. [DOI: 10.1117/1.OE.62.1.010902]

Keywords: fiber Bragg grating; pressure sensors; intrinsic sensitization; extrinsic sensitization; temperature compensation.

Paper 20220911V received Aug. 18, 2022; accepted for publication Dec. 30, 2022; published online Jan. 25, 2023.

1 Introduction

Pressure is one of the significant physical parameters strongly associated to life and production.[1] There are numerous methods for measuring pressure. Among them, pressure sensors are significant sensing devices that facilitate advancements in a variety of disciplines and advance society's intelligence. However, the majority of pressure sensors currently explored rely on capacitive, piezoelectric, and piezoresistive systems, which are vulnerable to electromagnetic interference. In addition, for multipoint pressure measurement, these sensors require an array design, resulting in a complex fabrication procedure. In addition, the array design increases the number of wires, which might lead to unequal current distribution and certain safety hazards in practical implementations.[2] Fiber Bragg grating (FBG) pressure sensors, on the other hand, employ gratings as sensing elements and may engrave many gratings on a single optical fiber, making multipoint distributed pressure measurements easier.[3,4] In addition, the FBG pressure sensor's strong antielectromagnetic interference capability and great safety are a result of its usage of optical signals for sensing. It is appropriate for pressure monitoring in areas with severe electromagnetic interference or dangerous conditions, such as the aircraft,[5,6] oil wells,[7–9] and pipelines.[10–14] In addition, FBG pressure sensors have been implemented in biological domains, such as blood pressure monitoring,[15–17] sleep quality monitoring,[18] and plantar pressure monitoring,[19–23] among others. It has significant consequences for medical diagnostics and rehabilitation[5,24–28] and also advances the prevention of diabetic lesions and prosthetic

*Address all correspondence to Hao Liu, liuhao@tiangong.edu.cn, Xiujuan Wang xjzwang@outlook.com

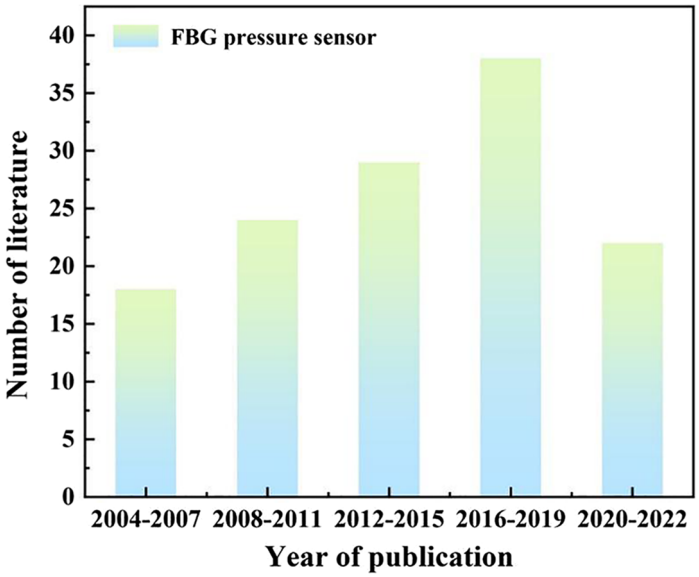

Fig. 1 Literature statistics for FBG pressure sensors.

development.[29,30] Research on FBG pressure sensors has increased in recent years, as shown in Fig. 1, since research on pressure sensors has received a great deal of attention, but there is still a big research opportunity for it.

For pressure sensitization of FBG pressure sensors, many scholars in China and abroad have conducted much research and proposed various sensitization methods. Some researchers have also conducted a review study of the work related to FBG pressure sensors. They have broadly classified FBG pressure sensors into polymer-encapsulated FBG pressure sensors, diaphragm-based FBG pressure sensors, and FBG pressure sensors of other structures according to the different types and structures of FBG packages.[3] FBG pressure sensors are classified into embedded FBG pressure sensors, pasted FBG pressure sensors, and suspended FBG pressure sensors.[31,32] However, these two standard classifications do not provide comprehensive coverage of the research related to FBG pressure sensors. Therefore, in this paper, we classify FBG pressure sensors into two categories, intrinsically sensitized FBG pressure sensors (sensitized by the characteristics of the optical fiber body) and extrinsically sensitized FBG pressure sensors (sensitized by an auxiliary device/mechanical structure other than the optical fiber body), based on the different sensitization methods of FBG pressure sensors, in order to cover all FBG pressure sensors related studies to the maximum extent. In addition, we propose a classification of externally sensitized FBG pressure sensors. The extrinsically sensitized FBG pressure sensors are classified into metal-mechanical structure-based FBG pressure sensors and polymer-mechanical structure-based FBG pressure sensors, i.e., from the point of view of the sensitizing material. This is because we found that different sensitized structures may use the same kind or type of sensitized materials, and the choice of sensitized materials is closely related to the pressure sensitization effect. These are the different aspects of our study.

The objective of this research is to examine recent developments in FBG pressure sensors. The optical transmission base of optical fiber and the FBG pressure sensing technique are described first. Then as depicted in Fig. 2, two types of sensitized FBG pressure sensors are discussed: intrinsically sensitized FBG pressure sensors and extrinsically sensitized FBG pressure sensors. Focus is placed on the sensitization mechanism of the sensor, and comparisons are made between the pressure measurement range, pressure sensitivity, and temperature sensitivity. Next, the pros and cons of various sensitization techniques for FBG pressure sensors are outlined. In conclusion, the current limits and potential trends of FBG pressure sensors are reviewed.

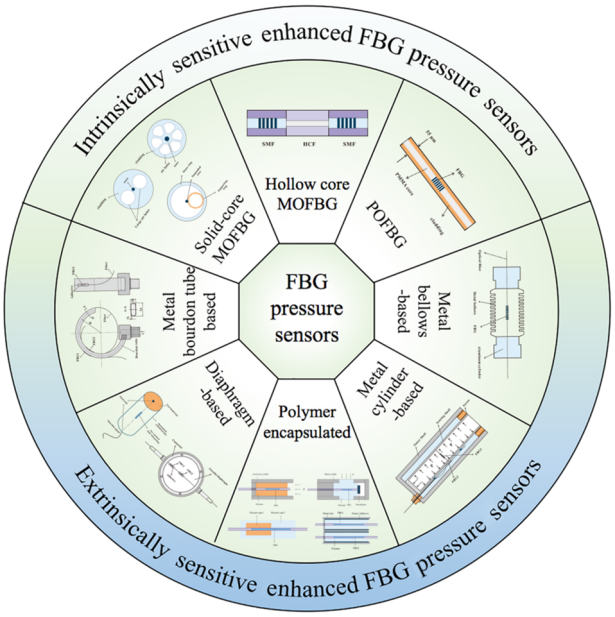

Fig. 2 The summary of FBG sensitivity enhancement methods.

2 Optical Transmission Basis of Optical Fiber and FBG Pressure Sensing Mechanism

As illustrated in Fig. 3(a), the optical fiber structure is simple and consists of three parts: coating, cladding, and core. For example, in a step-type single-mode fiber (SMF) (standard SMF), the outermost coating is used to protect the fiber. The innermost core is generally germanium doped, which makes the refractive index of the core slightly higher than that of the cladding, allowing light to advance by continuously generating total reflection at the intersection of the core and cladding, with the transmission mode of LP_{01} (fundamental mode), as shown in Fig. 3(b).

Germanium doping also imparts photosensitivity to the optical fiber core, allowing for the inscription of Bragg gratings. The refractive index of a photosensitive fiber core is modulated periodically by a Bragg grating.[34] An FBG corresponds to the formation of a narrowband (transmission or reflection) filter or reflector within a fiber core. As illustrated in Fig. 3(c), when broadband light flows through a fiber core with a Bragg grating, a selective reflection of narrowband light at a specific wavelength, known as the Bragg wavelength or central wavelength, is detected.

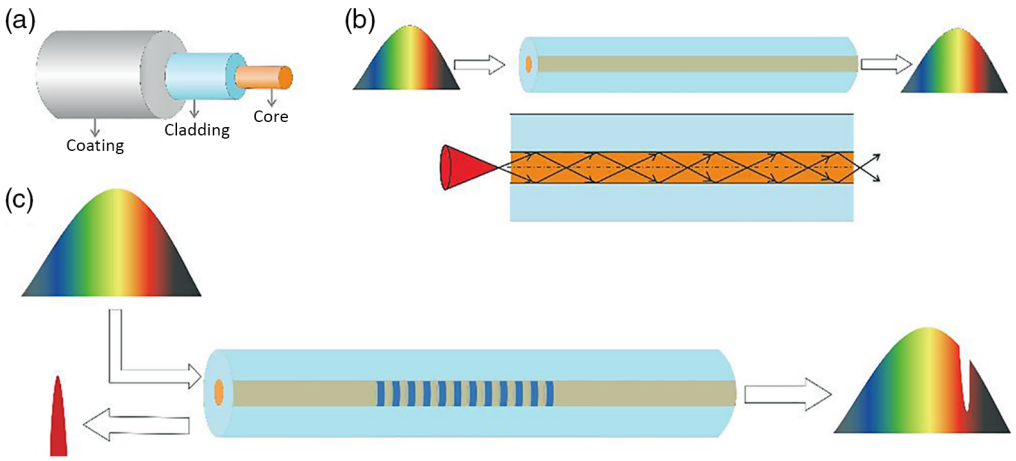

Fig. 3 (a)–(c) Working principle of FBG.[33] Copyright © 2022 MDPI.

The Bragg wavelength is given by[14]

$$\lambda_B = 2n_{\text{eff}}\Lambda, \tag{1}$$

where λ_B is the Bragg wavelength reflected by the Bragg grating, n_{eff} is the effective refractive index of the LP_{01} mode propagating in the fiber, and Λ is the grating period. FBGs are susceptible to external perturbations, such as temperature and strain. When the stress or temperature near the grating changes, the effective refractive index or the grating period shifts, causing a shift in the Bragg wavelength reflected. The Bragg wavelength shift is denoted by[14]

$$\frac{\Delta\lambda_B}{\lambda_B} = (1 - P_e)\varepsilon + (\zeta_f + \alpha_f)\Delta T, \tag{2}$$

where λ_B and $\Delta\lambda_B$ are the initial Bragg wavelength and its change, ε is the strain of the FBG, and ΔT is the temperature change of the FBG. P_e, ζ_f, and α_f are the photoelastic coefficient (theoretical value = 0.22), thermal-optic coefficient, and thermal expansion coefficient of the fiber, respectively. The FBG's reflected wavelength is affected by the intersection of strain and temperature, as shown by Eq. (2). Therefore, the temperature cross-sensitivity effect must be removed when measuring pressure utilizing the strain properties of fiber grating.[14]

When the external ambient temperature is constant, i.e. $\Delta T = 0$, Eq. (2) becomes Eq. (3, and Eq. (3) is as follows:

$$\frac{\Delta\lambda_B}{\lambda_B} = (1 - P_e)\varepsilon. \tag{3}$$

And from Refs. 35 and 36, it is known that

$$\varepsilon = \frac{\Delta L}{L} = -\frac{(1 - 2\mu)P}{E_f}, \tag{4}$$

where ΔL is the change in the physical length of the FBG, L is the original FBG physical length, E_f represents Young's modulus of the fiber, and μ represents the Poisson's ratio of the fiber.

Therefore

$$\frac{\Delta\lambda_B}{\lambda_B} = (1 - P_e)\left[-\frac{(1 - 2\mu)}{E_f}P\right]. \tag{5}$$

Based on Eq. (5), Young's modulus of the fiber[37] governs the pressure sensitivity of the FBG. Xu et al.[35] originally reported pressure sensing using a bare SiO_2 FBG and found a pressure sensitivity of −0.00304 pm/kPa. Bragg gratings inscribed on SiO_2 fibers have low-pressure sensitivity due to the high Young's modulus of SiO_2 (73.1 GPa).

3 Intrinsically Sensitive Enhanced FBG Pressure Sensors

Enhancing the intrinsic sensitivity of FBG pressure sensors by the use of the optical fiber body's features. Intrinsic sensitivity enhancement of FBG pressure sensors is mostly comprised of microstructured fiber Bragg grating (MOFBG) pressure sensors that utilize the internal microstructure of optical fibers to improve sensitivity and polymer fiber Bragg grating (POFBG) pressure sensors that improve sensitivity by decreasing the Young's modulus of the fiber material.

3.1 *MOFBG Pressure Sensors*

Russell e al. first introduced the concept of microstructured optical fiber (MOF) in 1992.[38] MOFs is a new type of fiber with a complex distribution of cross-sectional structures, also known as photonic crystal fibers (PCF). Knight et al.[39] first reported on the drawn MOF. Microstructured fibers are a technological breakthrough in fiber. MOFs have rapidly developed through continuous theoretical exploration and engineering practice. The fabrication process of MOFs is

complicated, generally through the traditional "stack-and-pull" technique, in which a stack of prefabricated fiber rods containing longitudinal capillaries is stretched longitudinally. The cross section of a successfully drawn microstructured fiber is a uniform distribution of air holes, and these holes are distributed periodically along the fiber direction. Because of the unique structure inside the microstructured fiber, this fiber has not only distinctive characteristics of traditional SiO_2 fiber, such as high birefringence characteristics but also overcomes many limitations inherent in traditional SiO_2 fiber, such as the flexibility to change the arrangement, size, shape, and spacing of the MOF cladding air holes to change its characteristics.

MOFs can be divided into two main categories according to different light-guiding principles. One kind is the solid core MOF with total internal reflection, which typically consists of a single medium (SiO_2) with several air holes consistently distributed in the cladding along the axial direction of the fiber. Conventional SiO_2 fiber requires germanium doping in the core to make the core's refractive index slightly greater than that of the cladding, resulting in total internal reflection and guiding light propagation within the core. Solid-core MOFs expose the cladding to air via microstructured holes, thereby lowering the cladding's refractive index and facilitating the propagation of light within the core. Eggleton et al.[40] were the first to successfully write FBGs on germanium-doped photosensitive MOF cores, marking a milestone in MOF sensing. By writing FBG on the MOF core, an MOFBG pressure sensor can be prepared. Utilizing the internal microstructure of MOF, the MOFBG pressure sensor is pressure sensitized. Due to the existence of large air holes in the MOF coating, which allows it to sustain a greater axial strain than SMF,[41] the pressure sensitivity of MOFBG is substantially greater than that of single-mode fiber bragg grating (SMFBG). Because distinct axial stresses are created on the MOF and SMF when axial pressure is applied to the fiber ends:

for MOF, the axial stress $\sigma_z = -\frac{A_0}{A_F} p$,

for SMF, the axial stress $\sigma_z = -p$,

where p is the applied pressure, A_0 is the total area of the MOF cross section, and A_F is the area of silica in the MOF cross section. Due to the presence of pores, A_0 is larger than A_F, and the axial stress σ_z on MOF is larger than the axial stress σ_z on SMF under the same axial pressure. Therefore, the pressure sensitivity of the MOFBG is larger than that of the SMFBG,[42] making the prospective pressure sensing applications of the MOFBG more relevant. Wu et al.[41,43] utilized a 193-nm excimer laser and a phase mask with a period of 1065 nm to write FBG into a grapefruit microstructured fiber (GMF) with a GMF cross section depicted in Fig. 4(a), and the measured pressure sensitivity was approximately three times that of SMFBG. Jewart et al.[44] wrote FBGs onto a dual-aperture fiber using an ultrafast laser. The core of the dual-aperture fiber is only 1 μm from the edge of one of the air holes, indicating that the air holes are large, as seen in Fig. 4(b), and that the larger air holes optimize the pressure sensitivity of the FBG. Htein et al.[45] presented two comparable single-ring suspension fibers, as depicted in Figs. 4(c) and 4(d), in which the cores are supported by a silicon ring and the entire structure is then enclosed by an annular ring. The air filling rate of MOF2 (65%) is significantly greater than that of MOF1 (44%). Therefore, the pressure sensitivity of MOF2 is significantly larger than that of MOF1, approximately twice as large, and the pressure sensitivities of the two MOFs are 6 and 11 times those of SMF, respectively, providing further evidence that an increase in cladding porosity increases pressure sensitivity. Sebastian et al.[46] analyzed the response of FBG written in a side-bore fiber to pressure by adjusting various parameters of the side-bore fiber, such as side-bore radius, side-bore spacing, fiber radius, fiber length, and encapsulation material, using a finite-element method. Also they verified this conclusion that increasing the hole radius would improve the FBG pressure sensitivity. In addition, it was found that shortening the side hole spacing, increasing the fiber radius (2.5 to 17.5 mm) and fiber length (10 to 30 mm), and selecting an encapsulation material with low Young's modulus within a specific range would also improve the pressure sensitivity of FBGs. This is due to the fact that materials with lower Young's modulus are more prone to pressure-induced deformation and hence more effectively transfer pressure to the fiber. Simulating the optimized parameters (hole spacing: 1000 μm, encapsulation material: RTV3145, hole radius: 8.25 mm, fiber radius: 17.5 mm, and fiber length: 30 mm,), the pressure sensitivity is as high as 280 pm/kPa. This is the highest pressure sensitivity reported for MOFBG, and its high-pressure sensitivity may be related to the larger air holes in the cladding and the low Young's modulus (1.1 MPa) of the encapsulation material is closely related.

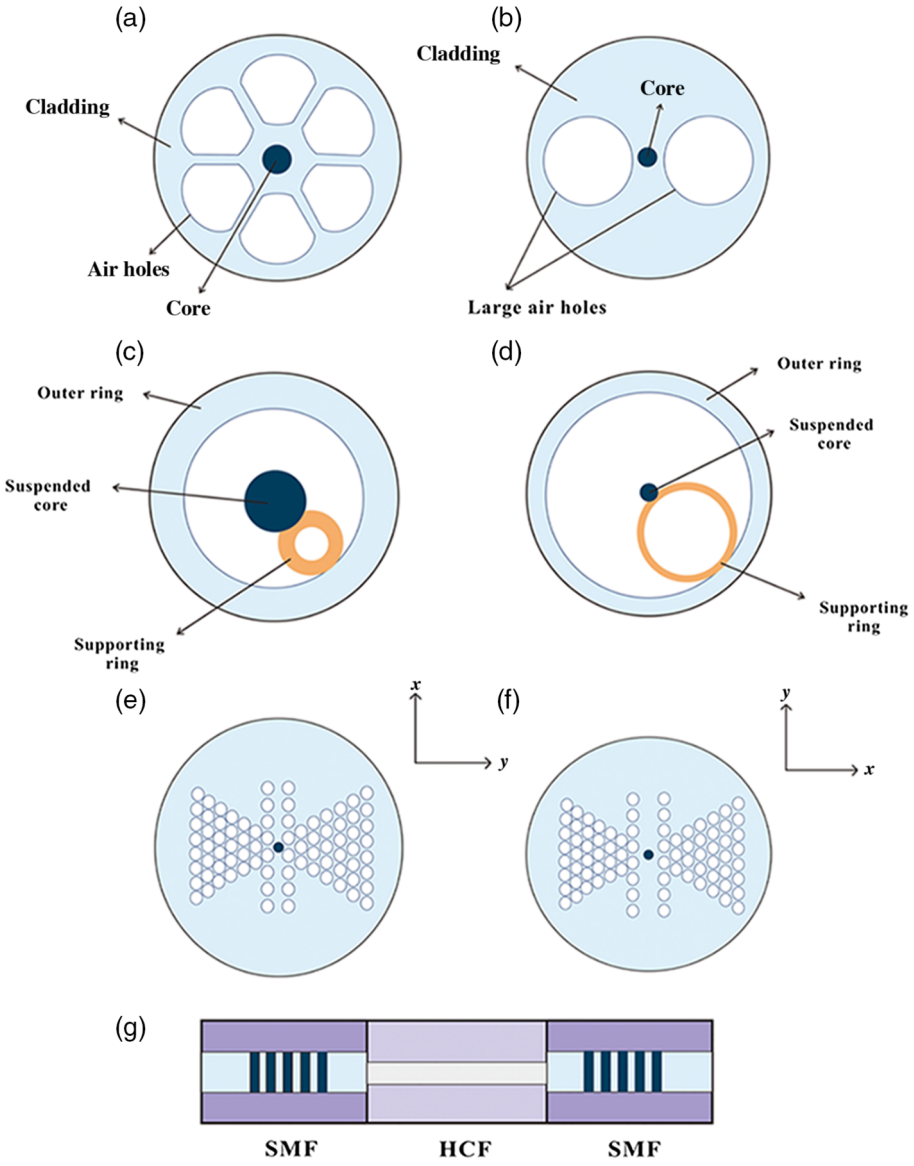

Fig. 4 Cross section of the (a) grapefruit MOFBG pressure sensor and (b) double-hole FBG pressure sensor. (c), (d) Cross section of the single-ring suspended FBG pressure sensor: (c) MOF1 and (d) MOF2. (e), (f) FBG in HB-MOF with air holes lattice pressure sensor arranged in (e) *y* direction and (f) *x* direction of the fiber. (g) SMF-HCF-SMF pressure sensor.

However, this is only a theoretical simulation value, and further experimental validation is needed.

Due to the fact that the asymmetry of MOF air holes can create birefringence, employing air holes of different sizes in two orthogonal directions of MOF or locally altering the geometry of the fiber core can make MOF very birefringent. High-pressure sensitivity has been reported for FBG etched on extremely birefringent MOF. Chen et al.[47] employed the phase mask approach to engrave polarization-maintaining FBG into HB-MOF. Due to the differing effective refractive indices of the two orthogonal polarization modes, the FBG produces two pressure-responsive reflection peaks at distinct wavelengths. Due to the presence of two borosilicate components adjacent to the fiber core, the MOF birefringence is as high as 7.2×10^{-4} and the pressure sensitivity is 0.020 pm/kPa, which is ~6.6 times greater than that of bare FBG. MOFs with elliptical cores show stronger birefringence compared to those with cylindrical cores. Chmielewska et al.[48] etched FBGs into side-hole fibers with elliptical cores and strong birefringence, therefore, increasing the pressure sensitivity to 0.00537 pm/kPa. Additionally, altering the arrangement

and size of stomata in asymmetric MOFs enhances the birefringence of MOFs. Sulejmani et al.[49] created FBGs in two MOFs with a strong birefringence. The layout and size of the stomata of these two MOFs differ. The stomatal puncta of MOF1 are positioned along the fiber y direction as shown in Fig. 4(e), whereas the stomatal puncta of MOF2 are arranged along the fiber x direction as shown in Fig. 4(f), and MOF2 has bigger stomatal size. Therefore, MOF2 possesses a greater birefringence than MOF1. Consequently, the pressure sensitivity of MOF2 (0.033 pm/kPa) is almost double that of MOF1 (−0.015 pm/kPa). Further evidence demonstrates that increasing the birefringence of MOF improves its pressure sensitivity.

Another type is photonic bandgap hollow-core MOF, which has a lot of air holes in the core and a refractive index that is lower than the cladding. The primary function of air core MOF is to direct light via the photonic band gap. Only light waves within the band gap are able to propagate through the air core, whereas light waves outside of the band gap are refracted into the cladding. Knight et al.[50] successfully fabricated an MOF with a photonic bandgap, confirming the photonic bandgap waveguide effect in optical fibers. Cregan et al.[51] introduced "air-core single-mode photonic bandgap fibers" in 1999. For pressure sensing, Luo et al.[52] fused SMF at both ends of a hollow core fiber (HCF) and then used line-by-line femtosecond laser etching to engrave FBGs in two SMF cores with a cavity length of 88.3 μm in the middle HCF, as depicted in Fig. 4(g), with a sensitivity of 1.22 pm/kPa for pressure, and Table 1 summarizes the reported MOFBG pressure sensor.

In conclusion, MOFBG pressure sensors can be made more sensitive in a number of ways, including by increasing the air pore size of the MOF coating or by increasing its birefringence. It also has a significant temperature sensitivity, so for pressure measurement, the MOFBG must be temperature compensated. In addition, MOF preparation is relatively challenging. The stacking approach was the first to be described, and it is now the simplest to apply and most used method for MOF preparation. By stacking round capillaries according to the desired MOF and then drawing the MOF at high temperature and low tension, this approach produces prefabricated rods. Due to the peculiarity of the MOF structure, however, the production procedure is difficult

Table 1 The summary reported MOFBG pressure sensors.

Refs.	Type	Material	Pressure range (kPa)	Pressure sensitivity (pm/kPa)	Temperature range (°C)	Temperature sensitivity (pm/°C)
42	FBG in PM-PCF	SiO_2	25,000	−0.00184	20 to 150	10.51
48	FBG in HB-SHF	SiO_2	15,000	0.00537	5 to 100	5.9
47	FBG in HB-OF with quasirectangle air holes	GeO_2, SiO_2	10,000	0.020	−20 to 80	8.8
49	FBG in HB-MOF	GeO_2, SiO_2	9000	−0.015 (MOF1), 0.033 (MOF2)	—	—
53	FBG in HB-MOF	SiO_2	140,000	0.033	55 to 280	11.9
46	FBG in SHF	SiO_2	10,000	280	—	—
44	FBG in double hole fiber	SiO_2	13,100	—	23 to 858	14.9
41 and 43	FBG in GMF	GeO_2, SiO_2	40,000	−0.00629 (small-hole GMF), −0.01286 (large-hole GMF)	20 to 200	—
45	FBG in single-ring suspended fiber	GeO_2, SiO_2	52,000	−0.0222 (MOF1), −0.0436(MOF2)	30 to 200	11.5(MOF1), 10.8(MOF2)
52	FBG in SMF-HCF-SMF	SiO_2	2250	1.22	25 to 95	8.92
54	FBG in SMF-HCBF-HCC	SiO_2	2000	−3.747	450 to 900	25.925

and preparation conditions are stringent and precise, hence limiting the preparation of MOFBG pressure sensors.

3.2 *POFBG Pressure Sensors*

Compared with SiO_2 fibers, polymer optical fibers (POFs) have the advantages of low Young's modulus, high flexibility, and biocompatibility. Peng et al.[55] first reported POFBG, and the attention of POF has gradually increased. Poly(methyl methacrylate) (PMMA) materials have the advantage of low cost and are often used to fabricate POFs. In addition, some other polymer materials, such as cyclic olefin copolymer (ZEONEX), polycarbonate (PC), poly(D, L-propyleneglycol) (PDLLA), and fluorinated polymers (CYTOP), can be used. However, so far, biocompatible and inexpensive PMMA materials are still the first choice for preparing POFBG sensors, which are mainly based on the UV photosensitivity of polymeric materials. Pure PMMA materials have low photosensitivity, which can be improved by doping with substances with high photosensitivity. In recent years, Ishikawa et al.[56] disclosed another POF with a fluorinated polymer as the core material, which not only has lower loss in the infrared and visible ranges but also possesses photosensitive capabilities. POFBG is primarily produced using the phase mask technique[24] and femtosecond laser point-by-point/line-by-line inscription.[56] The phase mask method is one of the most frequently employed techniques for encoding FBGs. The device is straightforward and stable, despite the fact that it requires a high level of zero-level mask rejection and that various phase masks are needed to create FBGs of various wavelengths. Femtosecond laser point-by-point/row-by-row etching gives versatility in grating shape and wavelength; however, grating preparation requires pricey femtosecond laser systems, and direct laser writing resolution limits the preparation of visible band gratings.

Writing FBG onto POF cores will enable the creation of POFBG pressure sensors. Due to POF's low Young's modulus, pressure sensors made of POFBG are pressure sensitized. This is because Young's modulus of the fiber controls the pressure sensitivity of FBG. The lower the Young's modulus of the fiber is, the higher the pressure sensitivity of the Bragg grating etched into it is. Since the Young's modulus of POF is 25 to 30 times less than that of SiO_2 fiber,[24,37,57] POF can offer greater pressure, which makes POF a potentially good candidate for pressure sensing applications.[37] Posttreatment, i.e., fiber thinning, can further reduce the Young's modulus of POF, hence enhancing its pressure sensitivity.[37] Etching with an acetone solution is one of the greatest ways to minimize the thickness of the POF cladding.[24] The thickness of the cladding etch depends on the acetone solution concentration and soaking duration.[24,37] Rajan et al.[24] put POF into a 1:1 combination of 99.5% acetone and methanol for 12 min in order to produce POF with a cladding diameter of 30 μm. Bhowmik et al.[37] put POF with a diameter of 180 μm into a 1:1 mixture of 99% acetone and methanol and etched it to a diameter of 130, 105, 80, and 55 μm at various immersion periods. As seen in Table 2, the pressure sensitivity of POFBG rises as the diameter of etched POF decreases. The pressure sensitivity of the 55-μm-diameter etched POFBG was 3.75 times that of the 243-μm- and 180-μm-diameter unetched POFBGs. This is

Table 2 The summary reported POFBG pressure sensors.

Refs.	Method	Material	Pressure range (kPa)	Pressure sensitivity (pm/kPa)	Temperature range (°C)	Temperature sensitivity (pm/°C)
37 and 58	243- and 180-μm unetched POFBGs	PMMA	1000	0.20	25 to 55	−95
37	130-μm etched POFBG	PMMA	1000	0.32	25 to 55	−120
37	105-μm etched POFBG	PMMA	1000	0.45	25 to 55	−136.7
37	80-μm etched POFBG	PMMA	1000	0.60	25 to 55	−153.3
37	55-μm etched POFBG	PMMA	1000	0.75	25 to 55	−170
56	PFGI-POF-FBG	PFGI	500	−0.13	—	—

due to the fact that when POF is immersed in the acetone solution, it absorbs a portion of the solution and relaxes the polymer chain tension. Since Young's modulus is proportional to stress ($E = \frac{\sigma}{\varepsilon}$), the stress reduction will eventually reduce Young's modulus and thus improve its pressure sensitivity. The Young's modulus of the etched POFBG with a 70-μm diameter was 0.85 GPa lower than that of the unetched POF with a 180-μm-diameter.[37] However, etching also raises the thermal expansion coefficient of the fiber, which significantly enhances the POFBG's temperature sensitivity. The temperature sensitivity of the etched 55-μm-diameter POFBG is increased by a factor of 1.8 when compared to the unetched 243- and 180-μm-diameter POFBGs. Therefore, temperature compensation of POFBG is necessary in order to measure pressure. The summary of reported POFBG pressure sensors is presented in Table 2.

In conclusion, the POFBG pressure sensor sensitization technique is extremely straightforward. Using a POF with a lower Young's modulus can increase pressure sensitivity, and the Young's modulus can be further lowered posttreatment to provide greater pressure sensitivity. However, the FBG inscription poses a hurdle for the POFBG pressure sensor. The phase mask method is the most often utilized grating inscription method at now. However, current commercial masks are developed for SiO_2 fibers, which require a significant change in the wavelength of the engraved light and are therefore ineffective for direct usage in POF. 193 or 248 nm is the typical wavelength of the light source for SiO_2 fibers, but 300 nm or higher is the norm for POF applications. The ideal phase mask should result in zero-level diffraction from the phase grating for a mask designed to engrave a grating with a 193- or 248-nm light source. In spite of the fact that research into POFBG inscription technology has advanced in recent years, it still lags behind SiO_2 optical fibers, which hinders the production of POFBG pressure sensors.

4 Extrinsically Sensitive Enhanced FBG Pressure Sensors

FBGs etched on ordinary SiO_2 fibers can also be made more sensitive by employing auxiliary devices or mechanical structures outside the fiber body to augment the pressure. These mechanical constructions are typically made of metals and plastics. This FBG pressure sensor type that requires a mechanical framework is known as an externally sensitized FBG pressure sensor.

4.1 *Metal Mechanical Structure-Based FBG Pressure Sensors*

Metal-based mechanical structures consist of metal diaphragms, metal spring tubes, metal bellows, and metal cylinders.

Diaphragms are thin, flexible sheets that deform under pressure and serve as a mechanical pressure amplifier. Round diaphragms are capable of greater deformation than square and rectangular diaphragms.[25] A diaphragm-based FBG pressure sensor is an FBG pasted radially to the center of a circular diaphragm,[25,59–61] sensing the strain ε_c in the center of the diaphragm under pressure, and can be expressed as

$$\varepsilon_c = \frac{3\sqrt{2}(1-\mu^2)R^2}{8Eh^2}P, \tag{6}$$

where E and μ are Young's modulus and Poisson's ratio of the diaphragm, respectively, and R and h are the radius and thickness of the diaphragm, respectively.

In case the temperature of the external environment is constant, the relationship between FBG wavelength change and strain is

$$\frac{\Delta\lambda_B}{\lambda_B} = (1-P_e)\varepsilon_c. \tag{7}$$

Therefore,

$$\frac{\Delta\lambda_B}{\lambda_B} = (1-P_e)\frac{3\sqrt{2}(1-\mu^2)R^2}{8Eh^2}P. \tag{8}$$

From Eq. (8), it can be seen that decreasing Young's modulus and the thickness of the diaphragm as well as increasing the diaphragm's radius can both increase the FBG's pressure sensitivity. Vaddadi et al.[62] tested the pressure sensitivity of FBG to various copper diaphragm thicknesses. With Young's modulus and the radius of the diaphragm held constant, a mere 0.2-mm reduction in diaphragm thickness enhanced the pressure sensitivity by 10.6 pm/kPa. Comparing Ref. 63 to Ref. 64, a 2-GPa reduction in Young's modulus increased the FBG pressure sensitivity by 0.3 pm/kPa for a fixed radius and thickness. However, a too-thin diaphragm cannot bear the high pressure, and a too-large diaphragm radius is impractical. Therefore, it is essential to select a diaphragm with a low Young's modulus.

As illustrated in Fig. 5(a), Huang et al.[65] adhered two FBGs with comparable beginning wavelengths along the radial direction to the surface of the stainless steel diaphragm for temperature compensation. FBG1 is close to the edge of the diaphragm (distance from the center point $R/\sqrt{3}$ to R) and senses only the radial strain ε_r in the diaphragm under pressure; ε_r can be expressed as

$$\varepsilon_r = \frac{3(1-\mu^2)(R^2-3r^2)}{8Eh^2}P. \tag{9}$$

FBG2 is attached to the center of the diaphragm for sensing the strain [as shown in Eq. (6)].

Since the FBG is sensitive to both temperature and strain, the FBG1 wavelength change versus strain and temperature is given by

$$\frac{\Delta\lambda_1}{\lambda_1} = (1-P_e)\frac{3(1-\mu^2)(R^2-3r^2)}{8Eh^2}P + (\zeta_f+\alpha_f)\Delta T. \tag{10}$$

FBG2 wavelength variation versus strain and temperature is as follows:

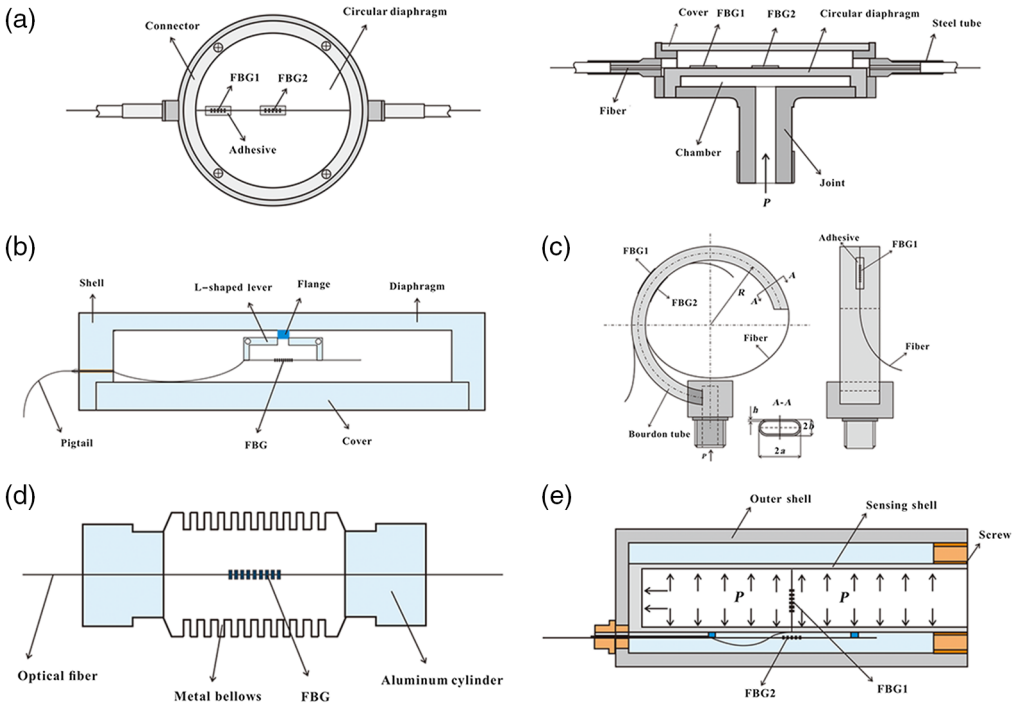

Fig. 5 Structure diagram of (a) a metal diaphragm-based FBG pressure sensor; (b) FBG earth pressure sensor combined with metal diaphragm and double L-shaped lever; and (c) metal spring tube-based FBG pressure sensor. (d) Metal bellows-based FBG pressure sensor structure diagram and (e) metal cylinder-based FBG pressure sensor structure diagram.

$$\frac{\Delta\lambda_2}{\lambda_2} = (1 - P_e)\frac{3\sqrt{2}(1-\mu^2)R^2}{8Eh^2}P + (\zeta_f + \alpha_f)\Delta T. \tag{11}$$

Due to the near proximity between FBG1 and FBG2, it may be assumed that the temperature-induced wavelength changes of both FBGs are identical. Equation (12) can be calculated from Eq. (11) minus Eq. (10), given that the beginning wavelengths of the two FBGs are comparable (assuming both initial wavelengths are λ) and the initial wavelengths are substantially bigger than the temperature/strain-induced wavelength change $\Delta\lambda$:

$$\Delta\lambda_2 - \Delta\lambda_1 = \frac{3\lambda(1 - P_e)(1-\mu^2)\left[\left(\sqrt{2}-1\right)R^2 + 3r^2\right]}{8Eh^2}P = kP, \tag{12}$$

where $k = \frac{3\lambda(1-P_e)(1-\mu^2)[(\sqrt{2}-1)R^2+3r^2]}{8Eh^2}$ is the pressure sensitivity coefficient, and r is a certain constant within $R/\sqrt{3}$ to R. Using the wavelength offset difference between the two FBGs as the sensing signal efficiently eliminates temperature cross sensitivity, as evidenced by Eq. (12). As high as 1.57 pm/kPa, the pressure sensitivity is about 513 times that of the FBG alone. The identical approach of temperature correction is also stated in Ref. 66.

Additionally, it has been stated that a metal diaphragm and a cantilever beam/fixed lever are coupled, with the diaphragm acting as a force collector.[6] Liang et al.[64] adhered two FBGs to the upper and lower surfaces of the cantilever beam and combined them with a stainless steel flat diaphragm and a force transmission rod enclosed in a protective sleeve. Under pressure, the plane diaphragm will deflect and turn into concentrated force. The transfer rod will exert a concentrated force on the cantilever beam to induce a wavelength change in the FBG, with a pressure sensitivity of 0.34 pm/kPa. The FBG was suspended from a double L-shaped lever, according to Li et al. As depicted in Fig. 5(b), the round stainless steel diaphragm was deformed under pressure, and the flange attached to its center would transfer the deformation. The double L-shape was able to transform longitudinal displacement into horizontal displacement, hence altering the FBG wavelength; the measured pressure sensitivity was 1.217 pm/kPa. The summary of metal diaphragm-based FBG pressure sensors is shown in Table 3.

There are numerous approaches to improve the sensitivity of FBG pressure sensors based on diaphragms. By decreasing Young's modulus and diaphragm thickness and increasing diaphragm radius, the pressure sensitivity of FBG can be enhanced. And the diaphragm-based FBG pressure sensor makes it simple to monitor multiple structures simultaneously. However, the adhesive attachment technique used for this type of pressure sensor, including uniformity, thickness, length, and width, as well as other characteristics, has a significant impact on the measurement accuracy. This is because the FBG must typically be attached to the diaphragm surface for sensitizing. In addition, to prevent the chirping phenomena, the strain distribution of FBG on the adhesion area must be uniform.

A spring tube (Bourdon tube) is a hollow metal tube with an oval or flat circular cross section that exhibits elastic deformation and mechanical pressure amplification under pressure. As depicted in Fig. 5(c), Huang et al.[10] bonded two FBGs with comparable initial wavelengths (set to λ_B) to the inner and outer sides of the spring tube, respectively. FBG1 is utilized to detect negative strain, whereas FBG2 is used to detect positive strain, as represented by Eqs. (13) and (14), respectively:

$$\frac{\Delta\lambda_{\mathrm{FBG1}}}{\lambda_{\mathrm{FBG1}}} = -(1 - P_e)\varepsilon_f + (\zeta_f + \alpha_f)\Delta T, \tag{13}$$

$$\frac{\Delta\lambda_{\mathrm{FBG2}}}{\lambda_{\mathrm{FBG2}}} = (1 - P_e)\varepsilon_f + (\zeta_f + \alpha_f)\Delta T, \tag{14}$$

$$\frac{\Delta\lambda_{\mathrm{FBG2}} - \Delta_{\mathrm{FBG1}}}{\lambda_B} = 2(1 - P_e)\varepsilon_f. \tag{15}$$

The approach avoids the wavelength shift induced by temperature fluctuations, successfully preventing temperature cross sensitivity, as demonstrated by Eq. (15). The strain is enhanced by

Table 3 The summary reported metal diaphragm-based FBG pressure sensors.

Refs.	Material	E_d (GPa)	R (mm)	H (mm)	Pressure range (kPa)	Pressure sensitivity (pm/kPa)	Temperature range (°C)	Temperature sensitivity (pm/°C)
59	Elastic metal film	206	7.5	2	60,000	0.0238	—	—
63	17-4PH Stainless steel	195	6	1	50,000	0.0357	−10 to 70	—
64	304 Stainless steel	193	6	1	10,000	0.34	5 to 70	—
66	Stainless steel	205	10	0.5	2000	1.03	0 to 60	—
65	304 Stainless steel	193	30	1.5	1000	1.57	20 to 90	—
67	193 Stainless steel	193	50	1	1000	2.02	—	—
68	Copper	117	30	0.5	965	2.96	—	—
69	6061 Aluminum	69	20	0.32	210	32.02	—	—
70	316 Stainless steel	28×10^6	72×72	0.4	689	0.0793	15 to 25	—
62	Copper	128	15	0.05, 0.25, 0.5	500	16.22, 5.609, 2.7802	—	—
62	304 Stainless steel	200	15	0.25, 0.5	500	2.63, 1.305	—	—
6	Stainless steel (APX-4)	211	12.5	2.02	70,000	0.0364	−40 to 90	21
60	Round film	—	15	0.1	10	—	—	—
71	Stainless steel	203	3.5	0.5	24	244	20 to 50	2.8
72	Stainless steel	203	100	5	2000	1.217	—	—
73	304 Stainless steel	193	Length15	0.5	2000	0.62271	27 to 62	19.672, 14.361

a factor of two compared to a single FBG, and the pressure sensitivity is up to 1.414 pm/kPa, which is 465 times that of a single FBG. In addition, by altering the spring tube's composition and shape, the sensor's pressure range and sensitivity can be better adjusted. However, the low stability of the spring tube, the sensor's vulnerability to external vibration, and the required high design precision have somewhat hampered the development of such sensors.

Metal bellows are an elastomeric element that is longitudinally deformable but not laterally deformable. Using this property of bellows, Song et al.[74] encased the FBG in a metal bellow, as depicted in Fig. 5(d). When the external pressure changes, the bellows will be forcibly elongated or contracted, resulting in a change in the grating pitch and the Elasto optic effect, which shifts the FBG wavelength and increases the pressure sensitivity to 48 pm/kPa.

The metal cylinder with narrow walls is also a pressure-sensitive element. Under external pressure, the cylinder deforms and can transform the pressure into a change in the cylinder's radial dimensions. Zhang et al.[75] took advantage of this property by adhering two FBGs to double-shell cylinders. As illustrated in Fig. 5(e), FBG1 is employed as a sensing grating, which is adhered to the tangential direction of the outer surface of the inner sensing cylinder to detect changes in temperature and pressure. Under the influence of internal pressure, the radial dimension of the sensing cylinder varies, resulting in axial strain in FBG1, and the FBG1 wavelength offset is proportional to the axial strain. As shown in the following equation:

$$\frac{\Delta\lambda_B^{S+T}}{\lambda_B} = (1 - P_e)\varepsilon + [\zeta_f + (1 - P_e)(\alpha_s - \alpha_f)]\Delta T, \tag{16}$$

where α_s is the coefficient of thermal expansion of the metal cylinder.

FBG2 is adhered to the axial direction of the outer surface of the inner sensing cylinder as a temperature compensation grating and solely detects temperature changes. The FBG2 wavelength offset is denoted by

$$\frac{\Delta\lambda_B^T}{\lambda_B} = [\zeta_f + (1 - P_e)(\alpha_s - \alpha_f)]\Delta T. \tag{17}$$

Since both FBGs are attached to the same metal cylinder, their temperature sensitivity is identical. By subtracting the center wavelengths of the two reflection peaks, it is possible to eliminate the influence of temperature variations on the pressure measurement and achieve temperature compensation with a pressure sensitivity of 0.0937 pm/kPa. Additionally, it was stated[76] that a birefringent FBG was sandwiched between an elastic cylinder high voltage transducer and an external protective sleeve. The FBG will create two reflection peaks at different wavelengths due to the various effective refractive indices of the two orthogonally polarized modes. Both reflection peaks move in opposite directions in response to pressure, yielding a pressure sensitivity of 0.027 pm/kPa. Wall metal cylinder-based FBG pressure sensors are often less sensitive, and it is difficult to guarantee the collimation of the glued optical fibers. Nonetheless, large-range measurements are simple to obtain, with good measurement precision, and it is simple to obtain a number of structural combinations of readings, which is a promising method for enhancing sensitivity. The summary of other metal structure FBG pressure sensors is presented in Table 4.

4.2 *Polymer Mechanical Structure-Based FBG Pressure Sensors*

Polymer diaphragms and coating/filling materials are frequently used in polymer mechanical structures. In comparison to metallic diaphragms, polymer diaphragms have a lower Young's modulus (0.0018 to 3.5 GPa),[81,82] which can greatly increase pressure sensitivity. In Fig. 6(a), Rajan et al.[24] illustrated how POFBG was vertically bonded to a thin vinyl diaphragm with a very low Young's modulus (2 to 2.5 GPa). The pressure sensitivity reached a maximum of 1320 pm/kPa, the greatest figure ever recorded for pressure sensitivity. Temperature correction

Table 4 The summary reported other metal structures FBG pressure sensors.

Refs.	Method	Material	Pressure range (kPa)	Pressure sensitivity (pm/kPa)	Temperature range (°C)	Temperature sensitivity (pm/°C)
10	FBGs bonded on Bourdon tube	Copper alloy	1000	1.414	—	—
77	FBGs bonded on metal bellows	Stainless steel	280	13.14	—	—
74	FBG bonded on metal bellows	Ti-5Al-2.5Sn alloy	100	48	—	—
75	Fags bonded on double shell cylinder	Stainless steel	4000	0.0937	10 to 60	20.3
78	Bonding of FBG to a magnetic transfer cantilever beam and diaphragm	304 Stainless steel	10	11.2	—	—
79	Double helix FBGs bonded on the metal disc substrate	Metal	5	36	—	—
80	FBG is encapsulated in a vacuum bellows and based on an iso-strength cantilever beam	Metal	130	100	10 to 40	—
76	FBG encapsulated in a free active cylinder bulk-modulus	Metal	100,000	0.027	24 to 30	—

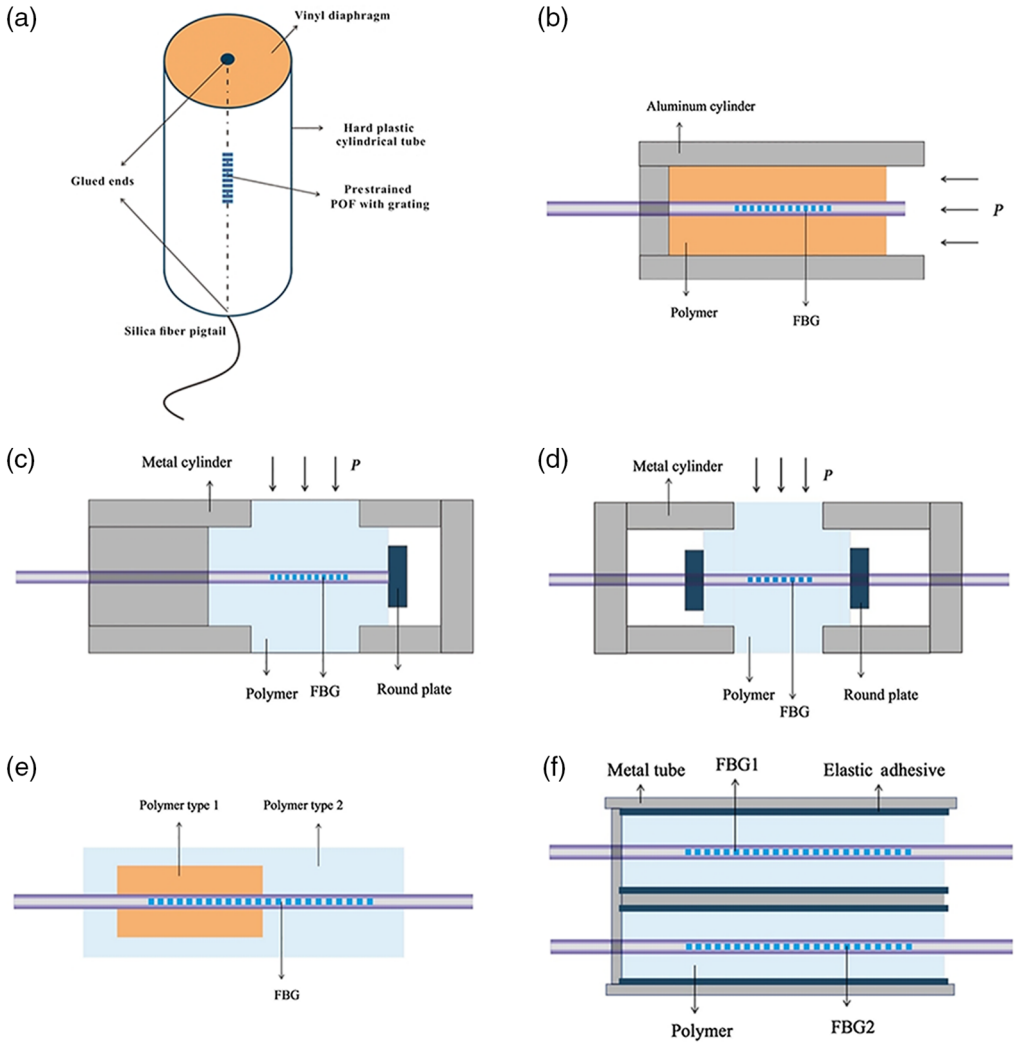

Fig. 6 (a) Polymer diaphragm-based POFBG pressure sensor. (b) FBG is encapsulated in a polymer-filled metal cylinder. (c) FBG is encapsulated in a polymer semifilled metal cylindrical pressure sensor with a circular plate fixed on one side of the polymer. (d) FBG is encapsulated in a polymer semifilled metal cylinder with circular plates fixed on both sides of the polymer. (e) FBG is encapsulated in two different polymers. (f) Polymer-encapsulated dual FBGs temperature and pressure sensor.

of the sensor is necessary due to the polymer diaphragm's high coefficient of thermal expansion, which also enhances the FBG's sensitivity to temperature. The list of reported polymer diaphragm-based FBG pressure sensors may be found in Table 5.

By coating the SiO_2 FBG with a polymer or embedding it into the polymer, Young's modulus E_f of the fiber will be completely neglected [as in Eq. (4)], and the strain ε acting on the fiber will be controlled by Young's modulus E_p of the polymer. The polymer used in this form of encapsulation has a low Young's modulus (0.0018 to 3.5 GPa),[81,82] which makes it an excellent way to increase the pressure sensitivity of naked FBGs. A 5-mm diameter polyurethane coating with a pressure sensitivity of −0.0652 pm/kPa, or nearly 21 times that of bare FBG, was applied to FBG in 1999 by Hill et al.[87]

The radial pressure will lessen the axial strain and refractive index alterations brought on by the axial pressure since the polymer-coated FBG will be subjected to the combined effect of the two pressures. To counteract the impact of radial pressure, Zhang et al.[88] enclosed the FBG in a thick-walled aluminum cylinder that was silicone rubber-cured. FBG was positioned on the axis of the cylinder and allowed to cure in the silicone rubber in a collimated state, as seen in Fig. 6(b).

Table 5 The summary reported polymer diaphragm-based FBG pressure sensors.

Refs.	Material	E_d (GPa)	R (mm)	h (mm)	Pressure range (kPa)	Pressure sensitivity (pm/kPa)	Temperature range (°C)	Temperature sensitivity (pm/°C)
25	Rubber	0.0014	14	0.125	15	116	—	—
83	Polyurethane rubber	0.012	4	1	200	7.23	—	—
84	Polyurethane	0.0067	20	—	1.2	370	20 to 50	20.3
85	Silicone rubber	0.0018	12.5	1	11.681	821.87	15 to 60	—
86	Silicone rubber	—	5.5	0.6	160	8.805	—	—
61	Epoxy resin	1.99	25	0.5, 0.7, 1.0	2.943	175.5, 89.5, 43.7	—	—
24	Etched POFBG on a vinyl diaphragm	2.5	4	0.06	0.79	1320	—	—

Only the pressure in the opening direction is permitted to create axial strain of the silicone rubber elastomer since the aluminum cylinder shields the pressure in all other directions, therefore, $\mu = 0$, Eq. (5) becomes

$$\frac{\Delta\lambda_B}{\lambda_B} = -\frac{(1 - P_e)}{E_p} P, \tag{18}$$

where E_p is Young's modulus of the polymer, and P is the pressure. The FBG only experiences axial pressure, which causes axial tensile strain, enhancing the pressure sensitivity because the aluminum cylinder shields the radial pressure. The pressure sensitivity is 1720 times greater than that of the bare FBG and reaches a maximum of −5.274 pm/kPa.

The axial strain of the polymer can also be amplified to increase the FBG pressure sensitivity. As seen in Fig. 6(c), Sheng et al.[82] enclosed the FBG in an aluminum cylinder that was partially filled with silicone rubber. In order to prevent the silicone rubber from being crushed in more than one radial direction, causing radial strain, two apertures were made on the opposing sides of the aluminum cylinder that contained the silicone rubber component. Equation (19) illustrates how the corresponding strain is also generated in the axial direction as a result of the Poisson's ratio effect:

$$\varepsilon_x = -\mu\varepsilon_y, \tag{19}$$

where ε_x is the axial strain, ε_y is the radial strain, and μ is the Poisson's ratio. Small pressures can produce substantial axial tensile strains in silicone rubber because of its extremely low stiffness (2 to 6 Mpa) and high Poisson's ratio, as well as the circular plate mounted to the material. When squeezed, the circular plate also consistently prevents slippage between the fiber and the polymer. This packaging technique has a pressure sensitivity of up to 33.876 pm/kPa, which is 10 900 times greater than that of plain FBG. As shown in Fig. 6(d), Huang and Liang[89] also created a similar construction by encasing the FBG in a copper cylinder that was only partially filled with silicone sealant. Even so, they fixed circular plates to the polymer's two surfaces, and the pressure sensitivity reached 29.488 pm/kPa—9700 times higher than that of naked FBG.

Temperature and strain/pressure changes will cause FBGs' wavelengths to alter because these factors are sensitive to both. A single FBG or dual FBGs are commonly employed to achieve separate measurements of strain/pressure and temperature in order to address the cross sensitivity of strain/pressure and temperature. A portion of the FBG (designated as FBG1) was embedded by Liu et al.[81] inside polycarbonate cubes with a high pressure and temperature sensitivity coefficient. As seen in Fig. 6(e), the complete FBG was then encased in a polytetrafluoroethylene cube. The other component of the FBG, designated as FBG2, encapsulates exclusively

with polytetrafluoroethylene. The polytetrafluoroethylene cube serves mostly as grating protection and has negligible impact on the FBG2's sensitivity to pressure and temperature. When the pressure and temperature change, two reflection peaks will arise because the FBGs at both ends are enclosed by different polymers. The following equation can be used to simultaneously determine the pressure and temperature by observing the shift in the center wavelength of these two reflection peaks:

$$\begin{pmatrix} \Delta\lambda_{B1}/\lambda_{B1} \\ \Delta\lambda_{B2}/\lambda_{B2} \end{pmatrix} = \begin{pmatrix} k_{p1} & k_{T1} \\ k_{p2} & k_{T2} \end{pmatrix} \begin{pmatrix} P \\ \Delta T \end{pmatrix}, \tag{20}$$

$$\begin{pmatrix} P \\ \Delta T \end{pmatrix} = \frac{1}{D} \begin{pmatrix} k_{T2} & -k_{T1} \\ -K_{p2} & -K_{p1} \end{pmatrix} \begin{pmatrix} \Delta\lambda_{B1}/\lambda_{B1} \\ \Delta\lambda_{B2}/\lambda_{B2} \end{pmatrix}, \tag{21}$$

where $D = k_{p1}k_{T2} - k_{T1}k_{p2}$, $\Delta\lambda_{B1}/\lambda_{B1}$, and $\Delta\lambda_{B2}/\lambda_{B2}$ are the relative wavelength shifts of FBG1 and FBG2, respectively. k_{p1} and k_{T1} are the pressure and temperature sensitivity coefficients of FBG1, respectively. k_{p2} and k_{T2} are the pressure and temperature sensitivity coefficients of FBG2, respectively.

Two FBGs were enclosed in a metal tube by Sun et al.,[90] as depicted in Fig. 6(f). FBG1 is a reference grating that solely detects temperature changes; pressure is unaffected. As a sensor grating, FBG2 is concurrently impacted by pressure and temperature. Temperature compensation is achieved by removing the impact of temperature variations on the pressure measurement through the subtraction of the wavelengths at the centers of the two reflection peaks.

The polymer-encapsulated FBG pressure sensor has a tiny, straightforward design that is capable of a wide dynamic range and good sensitivity. However, the encapsulation method needs to be improved because it is simple to apply uneven force to the FBG during the encapsulation process, leading to a chirp phenomena, for the FBG pressure sensor encased by polymer. The list of reported polymer-encapsulated FBG pressure sensors is summarized in Table 6.

5 Discussion

Both intrinsically and extrinsically sensitized FBG pressure sensors are examined in this review. The MOFBG and POFBG pressure sensors belong to the class of FBG pressure sensors that have a naturally higher sensitivity. According to different sensitizing materials, FBG pressure sensors with externally increased sensitivity can be separated into metal mechanical structure-based and polymer mechanical structure-based FBG pressure sensors. Each of these FBG pressure sensors has its advantages and disadvantages, with different sensitizing effects, ranges, and application areas, as shown in Fig. 7 and Table 7. High pressure ($\geq$1000 kPa) measurements are possible because to the wide pressure measurement range of MOFBG pressure sensors, metal diaphragm-based FBG pressure sensors, and polymer-encapsulated FBG pressure sensors. Other FBG pressure sensors, in comparison, have a smaller pressure measurement range and are better suited for readings of medium pressure ($>$10 kPa) and low pressure ($\leq$10 kPa). The polymer diaphragm-based FBG pressure sensor, followed by the metal diaphragm-based FBG pressure sensor, has the best sensitization effect from the standpoint of increasing sensitivity. The FBG pressure sensor built from a metal cylinder has the worst sensitization effect.

The reference grating and dual-grating difference output methods are the most frequently utilized temperature compensation techniques.[4] In order to guarantee that any temperature change will have the same effect on both FBGs, the reference grating method includes installing two FBGs with identical performance in a temperature-controlled environment. One of the FBGs is used as a reference grating, which senses just temperature changes without pressure, to detect ambient temperature changes. In contrast, the other FBG is used as a sensing grating subject to temperature and pressure. Temperature compensation is accomplished by subtracting the wavelength shift produced by the change in temperature from the total wavelength shift measured by the measuring grating. Temperature compensation is implemented chiefly using the reference FBG method for polymer-encapsulated FBG pressure sensors and metal cylinder-based FBG pressure sensors. The dual-grating difference output method involves adhering

Table 6 The summary reported polymer encapsulated FBG pressure sensors.

Refs.	Method	Material	Size (mm)	E_p (GPa)	μ	Pressure range (kPa)	Pressure sensitivity (pm/kPa)	Temperature range (°C)	Temperature sensitivity (pm/°C)
90	Double FBGs encapsulated in epoxy resin	Epoxy resin	—	—	—	20,000	0.044	20 to 100	0.0501
87	Polyurethane coated FBG	Polyurethane	$d = 5$	1.0	0.45	3450	−0.0652	—	—
88	FBG encapsulated in a silicone rubber-filled aluminum casing	Silicone rubber	$d = 11$	0.19	—	440	−5.28	—	—
91	FBG encapsulated in a silicone rubber compound-filled aluminum casing	Silicone rubber	$d = 20$	0.135	—	340	8.70	—	—
82	FBG encapsulated in a silicone rubber-halted-filled aluminum cylinder	Silicone rubber	$d = 11$	1.8×10^{-3}	0.4	200	33.876	—	—
92 and 93	FBG embedded in silicone rubber	Silicone rubber	$d = 4$	2 to 6×10^{-3}	0.4 to 0.5	—	−0.02128	−100 to 320	—
94	FBG embedded in silicone rubber	Silicone rubber	$d = 3$	—	—	100	0.026	0 to 35	13
95	FBG encapsulated in a polymer-filled metal casing	Polymer	—	—	—	240	14.92	—	—
96	FBG encapsulated in a polymer cuboid	Polymer	$10 \times 15 \times 50$	3.5	0.35	10,000	0.09576	0 to 80	80.465
97	SFBG encapsulated in a polymer-halted-filled metal cylinder	Polymer	—	—	—	160	45	20 to 80	23
98	FBG encapsulated in a polymer-halted-filled metal cylinder	Polymer	—	—	—	7.16	149.5	—	—
81	FBG embedded in polycarbonate cube	Polycarbonate	$5 \times 5 \times 50$	3.5×10^{-18}	0.35	10,000	−0.08056	~80	88.825
89	FBG encapsulated in a silicone sealant-halted-filled copper cylinder	Silicone sealant	—	—	—	240	29.488	0 to 75	—
99	FBG encapsulated in a silicone sealant-halted-filled stainless steel pipe	Silicone sealant	$d = 0.2$	3.72×10^{-4}	0.49	250	0.0587	—	—
100	FBG encapsulated in a silicone sealant-halted-filled stainless steel pipe	Silicone sealant	$d = 0.4$	—	—	1630	—	—	—

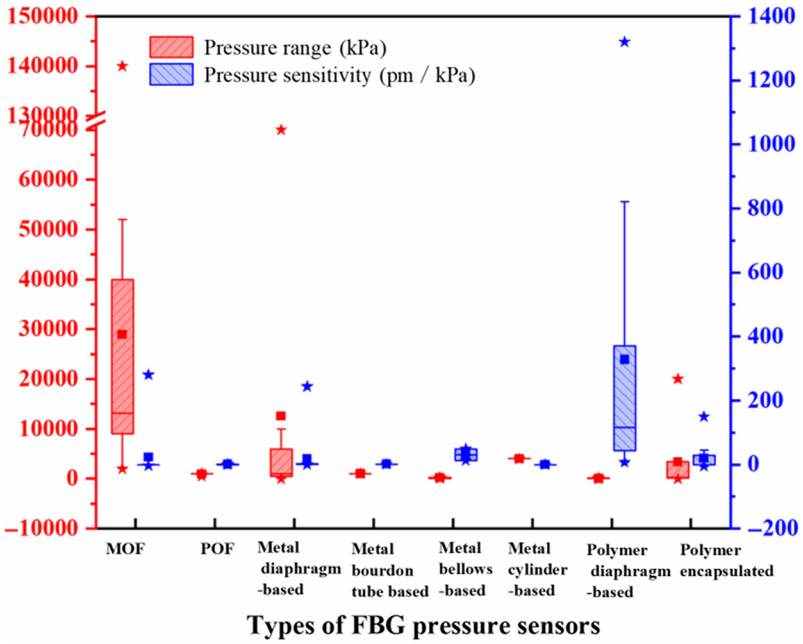

Fig. 7 Performance comparison of FBG pressure sensors.

two FBGs with the same performance to the corresponding portions of the mechanical structure and measuring the positive and negative stresses on the surface of the mechanical structure when it is elastically deformed under the observed pressure. The effect of ambient temperature on the two FBGs can be deemed equivalent. The difference between the wavelength shifts of these two FBGs can eliminate temperature cross sensitivity, thereby improving the FBG's measurement sensitivity. Temperature compensation is achieved primarily by the dual-grating difference output method in diaphragm-based FBG pressure sensors and metal spring tube-based FBG pressure sensors.

For MOFBG pressure sensors, the difficulty lies in the preparation of MOF, which is generally made by the traditional "stack-and-pull" technique, in which a stack of prefabricated optical fiber rods containing longitudinal capillaries is stretched longitudinally.[101] Due to the peculiarity of the MOF structure, however, the production procedure is difficult and preparation conditions are stringent and precise, hence limiting the preparation of MOFBG pressure sensors. The FBG inscription poses a hurdle for the POFBG pressure sensor. The phase mask method is the most often utilized grating inscription method at now. However, current commercial masks are developed for SiO_2 fibers, which require a significant change in the wavelength of the engraved light and are therefore ineffective for direct usage in POF. 193 or 248 nm is the typical wavelength of the light source for SiO_2 fibers, but 300 nm or higher is the norm for POF applications.[101] The ideal phase mask should result in zero-level diffraction from the phase grating for a mask designed to engrave a grating with a 193- or 248-nm light source. In spite of the fact that research into POFBG inscription technology has advanced in recent years, it still lags behind SiO_2 optical fibers, which hinders the production of POFBG pressure sensors. The preparation process is more advanced for externally sensitized FBG pressure sensors. For diaphragm-based FBG pressure sensors, metal spring tube-based FBG pressure sensors, and metal cylinder-based FBG pressure sensors, the FBG is typically sensitized by being adhered to the surface of the mechanical structure. However, the adhesive attachment technique used for this type of pressure sensor, including uniformity, thickness, length, and width, as well as other characteristics, has a significant impact on the measurement accuracy. In addition, to prevent the chirping phenomena, the strain distribution of FBG on the adhesion area must be uniform. It is necessary to enhance the encapsulation process for polymer-encapsulated FBG pressure sensors since it can cause uneven stress on the FBG and the chirping phenomena.

In terms of application, MOFBG pressure sensors are composed of high-temperature resistant SiO_2 and have an extensive range, so they can be used for static high-pressure measurements

Table 7 Comparison of several FBG pressure sensors.

Type			Advantages	Drawbacks	Application	Temperature compensation
Intrinsically sensitive enhanced FBG pressure sensors	MOFBG pressure sensors		More flexible sensitization method, large range, better sensitization effect, can realize multiparameter measurement	MOF preparation process is more complex	Oil and energy industries	—
	POFBG pressure sensors		High flexibility and biocompatibility, simple sensitization method, good sensitization effect by combination with mechanical structure	Poor heat resistance, POFs inscription technology lags behind SiO_2 optical fibers	Biomedical field	—
Extrinsically sensitive enhanced FBG pressure sensors	Metal-mechanical FBG pressure sensors	Metal diaphragm-based FBG pressure sensors	Sensitization method is more flexible, easy to achieve a variety of structure combination measurement, large range, better sensitization effect	Easy to chirp, susceptible to oxidation	Civil engineering, oil, gas, and aerospace industries	The dual-grating difference output method
		Metal spring tube-based FBG pressure sensors	By altering the spring tube's composition and shape, the sensor's pressure range and sensitivity can be better adjusted	The low stability of the spring tube, the sensor's vulnerability to external vibration. Susceptible to oxidation	Suitable for static pressure measurement of gases or liquids	The dual-grating difference output method
		Metal bellows-based FBG pressure sensors	Various combinations of structures can be realized for pressure sensitization	Small measuring range, easy to be oxidized	Suitable for low-pressure measurement of gases or liquids	—
		Metal cylinder-based FBG pressure sensors	Various combinations of structures can be realized for pressure sensitization	Poor sensitization effect; collimation of the fiber is not easy to ensure when pasting; not easy to connect the sensors in series	Suitable for high pressure measurement of gases	The reference grating method
	Polymer-mechanical FBG pressure sensors	Polymer diaphragm-based FBG pressure sensors	The sensitization method is more flexible, and the sensitization effect is good	Easy to chirp; polymer diaphragms are susceptible to corrosion and have poor high-temperature stability	Can be used for liquid level measurement, hydrophone detection and related fields, and biomedical field	The dual-grating difference output method
		Polymer encapsulated FBG pressure sensors	Simple structure, small size, large measuring range	Polymers are prone to aging and deterioration in high-temperature environments resulting in poor long-term stability of the sensor; easy to chirp	Biomedical, smart structures, oil, and gas industries	The reference grating method

of gases or liquids in high-temperature environments and have many potential applications in the petroleum and energy industries. POF is highly flexible and biocompatible, so POFBG pressure sensors are suitable for human health monitoring in biomedical fields, such as plantar pressure monitoring, which brings new advances in preventing diabetic lesions and enhancing prosthesis development. Research on POFBG pressure sensors has accelerated in recent years, but the current POF inscription technology still lags behind SiO_2 optical fibers. Compared with polymer mechanical structure-based FBG pressure sensors, metal mechanical structure-based FBG pressure sensors are more suitable for pressure monitoring in high-temperature and high-chemical corrosion harsh environments and have many potential applications in quasidistributed pressure measurements in civil engineering, oil, and gas fields. However, the durability is also somewhat limited by the oxidation of the metal during long-term use. Polymer mechanically based FBG pressure sensors, on the other hand, are less advantageous in industrial pressure measurement due to poor sensor stability caused by easy aging and deterioration in high-temperature environments. Polymer-encapsulated FBG pressure sensors have many potential applications in the biomedical field due to their simple structure and small size, which can achieve an extensive range and high sensitivity.

In conclusion, the above FBG pressure sensors have advantages and disadvantages. Metal-mechanical structure-based FBG pressure sensors are a good choice for pressure monitoring in harsh environments, such as high temperatures and strong corrosion. POFBG pressure sensors and polymer-encapsulated FBG pressure sensors have broad application prospects in biomedical fields due to their simple structure, small size, and good biocompatibility.

6 Conclusion and Outlook

Intrinsically and extrinsically sensitized FBG pressure sensors, two popular types of FBG pressure sensors, are covered in this review. The sensitization mechanisms and temperature compensation techniques of these FBG pressure sensors are highlighted, and their ranges, sensitization effects, pros and cons, and application fields are compared. Although FBG pressure sensors are frequently used in real-world settings, there is still room for development. The following are expected developments for the FBG pressure sensor.

(1) *Creating new materials and structures to increase sensitivity.* FBG pressure sensing technology has increasingly matured as a result of the FBG pressure sensors' rapid development in recent decades, particularly the sensor structure for increased sensitivity. Future research could focus on creating sensitizing materials as a means of improving FBG pressure sensing technology.

(2) *The creation and use of inexpensive FBG pressure sensors*. Inherent benefits of FBG pressure sensors are their resistance to electromagnetic interference, high level of safety, and simplicity of multipoint dispersed measurement. However, it costs a lot to produce such FBG pressure sensors right now. Reducing the price of FBG pressure sensors is an essential and fundamental requirement for widespread application, given their popularity and application.

(3) *The creation and use of different sensitization structures in conjunction with FBG pressure sensors*. New combined FBG pressure sensors with improved performance can be created by combining several sensitization structures. The designed combination FBG pressure sensor should have as few intermediary force transmission structures as practical, given its precision. Errors will accumulate due to the growth of intermediate force transmission mechanisms. Consequently, the new combined FBG pressure sensor should have a straightforward form. One potential for the future is the creation of coupled FBG pressure sensors with numerous sensitization structures.

(4) *Constructing and using a multiparameter FBG pressure sensor.* The majority of applications nowadays require obtaining numerous physical factors, such as pressure or removing interference from other physical values. In practical applications, it might be a good idea to test numerous physical parameters at once using multiparameter FBG sensors to streamline the measurement system.

Acknowledgments

This work was supported by the National Natural Science Foundation of China (Grant No. 51473122), the China Postdoctoral Science Foundation (Grant No. 2016M591390), and the National Key Research and Development Program "Winter Olympics of Science and Technology" Key Special Project (Grant No. 2019YFF0302105).

References

1. P. Song et al., "Recent progress of miniature MEMS pressure sensors," *Micromachines* **11**(1), 56 (2020).
2. X. Niu et al., "Fructus xanthii-inspired low dynamic noise dry bioelectrodes for surface monitoring of ECG," *ACS Appl. Mater. Interfaces* **14**(4), 6028–6038. (2022).
3. E. Vorathin et al., "Review of high sensitivity fibre-optic pressure sensors for low pressure sensing," *Opt. Laser Technol.* **121**, 105841 (2020).
4. Y. Kuang et al., "Packaging and temperature compensation of fiber Bragg grating for strain sensing: a survey," *Photonic Sens.* **8**(4), 320–331 (2018).
5. V. Neeharika and P. K. Pattnaik, "Optical MEMS pressure sensors incorporating dual waveguide Bragg gratings on diaphragms," *IEEE Sens. J.* **16**(3), 681–687 (2016).
6. G. Hegde, M. V. N. Prasad, and S. Asokan, "Temperature compensated diaphragm based fiber Bragg grating (FBG) sensor for high pressure measurement for space applications," *Microelectron. Eng.* **248**, 111615 (2021).
7. C. Holmes, J. C. Gates, and P. G. R. Smith, "Integrated optical differential pressure transducers achieved using thin buckled silica membranes and direct UV written planar Bragg gratings," *Sens. Actuators A: Phys.* **168**(1), 14–21 (2011).
8. H. Zhang et al., "Numerical and experimental studies of high-sensitivity plug-in pressure sensor based on fiber Bragg gratings," *Opt. Eng.* **55**(9), 096104 (2016).
9. Y. Sun, Q. Li, and C. Fan, "Laboratory core flooding experiments in reservoir sandstone under different sequestration pressures using multichannel fiber Bragg grating sensor arrays," *Int. J. Greenhouse Gas Control* **60**, 186–198 (2017).
10. J. Huang et al., "A fiber Bragg grating pressure sensor and its application to pipeline leakage detection," *Adv. Mech. Eng.* **5**, 590451 (2015).
11. Y.-L. Bai et al., "Simultaneous measurement of pressure and temperature based on processed capillary tube and fiber Bragg grating," *Opt. Eng.* **55**(8), 080502 (2016).
12. J. Wang et al., "Novel negative pressure wave-based pipeline leak detection system using fiber Bragg grating-based pressure sensors," *J. Lightwave Technol.* **35**(16), 3366–3373 (2017).
13. L. Zhang et al., "Performance investigation on pressure sensing from fiber Bragg grating loop ring-down cavity," *Opt. Commun.* **469**, 125759 (2020).
14. X. Liu et al., "Sensitivity-enhanced fiber Bragg grating pressure sensor based on a diaphragm and hinge-lever structure," *IEEE Sens. J.* **21**(7), 9155–9164 (2021).
15. Y. Katsuragawa and H. Ishizawa, "Non-invasive blood pressure measurement by pulse wave analysis using FBG sensor," in *Proc. IEEE Int. Instrum. and Meas. Technol. Conf. (I2MTC)*, 11–14 May 2015, Pisa, Italy, pp. 511–515 (2015).
16. U. Sharath et al., "Blood pressure evaluation using sphygmomanometry assisted by arterial pulse waveform detection by fiber Bragg grating pulse device," *J. Biomed. Opt.* **18**(6), 067010 (2013).
17. N. V. Kumar et al., "Fiber Bragg grating-based pulse monitoring device for real-time non-invasive blood pressure measurement—a feasibility study," *IEEE Sens. J.* **21**(7), 9179–9185 (2021).
18. L. Dziuda et al., "Fiber Bragg grating-based sensor for monitoring respiration and heart activity during magnetic resonance imaging examinations," *J. Biomed. Opt.* **18**(5), 057006 (2013).
19. D. Vilarinho et al., "POFBG-embedded cork insole for plantar pressure monitoring," *Sensors* **17**(12), 2924 (2017).
20. R. Suresh et al., "Development of a high resolution plantar pressure monitoring pad based on fiber Bragg grating (FBG) sensors," *Technol. Health Care* **23**(6), 785–794 (2015).

21. T. C. Liang, J. J. Lin, and L. Y. Guo, "Plantar pressure detection with fiber Bragg gratings sensing system," *Sensors* **16**(10), 1766 (2016).
22. Y.-F. Zhang et al., "A fiber Bragg grating based sensing platform fabricated by fused deposition modeling process for plantar pressure measurement," *Measurement* **112**, 74–79 (2017).
23. R. A. Lakho et al., "A smart insole for monitoring plantar pressure based on the fiber Bragg grating sensing technique," *Textile Res. J.* **89**(17), 3433–3446 (2019).
24. G. Rajan et al., "High sensitivity force and pressure measurements using etched single-mode polymer fiber Bragg gratings," *IEEE Sens. J.* **13**(5), 1794–1800 (2013).
25. G. Allwood et al., "A highly sensitive fiber Bragg grating diaphragm pressure transducer," *Opt. Fiber Technol.* **25**, 25–32 (2015).
26. K. Imade et al., "Measurement of sound pressure and temperature in tissue-mimicking material using an optical fiber Bragg grating sensor," *J. Med. Ultrason.* **43**(4), 473–479 (2016).
27. S. Poeggel et al., "Femtosecond-laser-based inscription technique for post-fiber-Bragg grating inscription in an extrinsic Fabry–Perot interferometer pressure sensor," *IEEE Sens. J.* **16**(10), 3396–3402 (2016).
28. N. Dong et al., "Pressure and temperature sensor based on graphene diaphragm and fiber Bragg gratings," *IEEE Photonics Technol. Lett.* **30**(5), 431–434 (2018).
29. E. A. Al-Fakih et al., "The capability of fiber Bragg grating sensors to measure amputees' trans-tibial stump/socket interface pressures," *Sensors* **13**(8), 10348–10357 (2013).
30. E. A. Al-Fakih et al., "Development and validation of fiber Bragg grating sensing pad for interface pressure measurements within prosthetic sockets," *IEEE Sens. J.* **16**(4), 965–974 (2016).
31. J. T. Lin et al., "Research progresses and developing trends of optical fiber grating pressure sensor," *Opt. Instrum.* **39**(1), 88–94 (2017).
32. B. H. Lin and Q. F. Shang, "Progress in improving pressure sensitivity of fiber Bragg grating sensor," *Opt. Commun. Technol.* **34**(2), 42–45 (2010).
33. X. Wang et al., "Fiber Bragg grating-based smart garment for monitoring human body temperature," *Sensors* **22**(11), 4252 (2022).
34. K. O. Hill et al., "Photosensitivity in optical fiber waveguides: application to reflection filter fabrication," *Appl. Phys. Lett.* **32**(10), 647–649 (1978).
35. M. G. Xu et al., "Optical in-fibre grating high pressure sensor," *Electron. Lett.* **29**(4), 398 (1993).
36. G. B. Hocker, "Fiber-optic sensing of pressure and temperature," *Appl. Opt.* **18**(9), 1445–1448 (1979).
37. K. Bhowmik et al., "Experimental study and analysis of hydrostatic pressure sensitivity of polymer fibre Bragg gratings," *J. Lightwave Technol.* **33**(12), 2456–2462 (2015).
38. P. St. J. Russell et al., "Recent progress in photonic crystal fibers," in *Proc. Opt. Fiber Commun. Conf.*, pp. 98–100 (2000).
39. J. C. Knight et al., "All-silica single-mode optical fiber with photonic crystal cladding," *Opt. Lett.* **21**(19), 1547–1549 (1996).
40. B. J. Eggleton et al., "Grating resonances in air–silica microstructured optical fibers," *Opt. Lett.* **24**(21), 1460–1462 (1999).
41. C. Wu, Y. Zhang, and B. -O. Guan, "Simultaneous measurement of temperature and hydrostatic pressure using Bragg gratings in standard and grapefruit microstructured fibers," *IEEE Sens. J.* **11**(2), 489–492 (2011).
42. G. Bai-Ou et al., "Bragg gratings in pure-silica polarization-maintaining photonic crystal fiber," *IEEE Photonics Technol. Lett.* **20**(23), 1980–1982 (2008).
43. C. Wu et al., "Characterization of pressure response of Bragg gratings in grapefruit microstructured fibers," *J. Lightwave Technol.* **28**(9), 1392–1397 (2010).
44. C. M. Jewart et al., "Ultrafast femtosecond-laser-induced fiber Bragg gratings in air-hole microstructured fibers for high-temperature pressure sensing," *Opt. Lett.* **35**(9), 1443–1445 (2010).
45. L. Htein et al., "Single-ring suspended fiber for Bragg grating based hydrostatic pressure sensing," *Opt. Express* **27**(7), 9655–9664 (2019).

46. S. Sebastian et al., "Highly sensitive fiber Bragg grating-based pressure sensor using side-hole packaging," *Appl. Opt.* **58**(1), 115–121 (2019).
47. G. Chen et al., "Simultaneous pressure and temperature measurement using Hi-Bi fiber Bragg gratings," *Opt. Commun.* **228**(1–3), 99–105 (2003).
48. E. Chmielewska, W. Urbanczyk, and W. J. Bock, "Measurement of pressure and temperature sensitivities of a Bragg grating imprinted in a highly birefringent side-hole fiber," *Appl. Opt.* **42**(31), 6284–6291 (2003).
49. S. Sulejmani et al., "Control over the pressure sensitivity of Bragg grating-based sensors in highly birefringent microstructured optical fibers," *IEEE Photonics Technol. Lett.* **24**(6), 527–529 (2012).
50. J. C. Knight et al., "Photonic band gap guidance in optical fibers," *Science* **282**(5393), 1476–1478 (1998).
51. R. F. Cregan et al., "Single-mode photonic band gap guidance of light in air," *Science* **285**(5433), 1537–1539 (1999).
52. J. Luo et al., "Phase-shifted fiber Bragg grating modulated by a hollow cavity for measuring gas pressure," *Opt. Lett.* **45**(2) 507–510 (2020).
53. J. Y. Huang et al., "FBGs written in specialty fiber for high pressure/high temperature measurement," *Opt. Express* **25**(15), 17936–17947 (2017).
54. Y. Wang et al., "Hollow core Bragg fiber integrated with regenerate fiber Bragg grating for simultaneous high temperature and gas pressure sensing," *J. Lightwave Technol.* **39**(17), 5643–5649 (2021).
55. G. D. Peng, Z. Xiong, and P. L. Chu, "Photosensitivity and gratings in dye-doped polymer optical fibers," *Opt. Fiber Technol.* **5**(2), 242–251 (1999).
56. R. Ishikawa et al., "Pressure dependence of fiber Bragg grating inscribed in perfluorinated polymer fiber," *IEEE Photonics Technol. Lett.* **29**(24), 2167–2170 (2017).
57. G. Woyessa et al., "Enhanced pressure and thermal sensitivity of polymer optical fiber Bragg grating sensors," *Opt. Laser Technol.* **130**, 106357 (2020).
58. K. Bhowmik et al., "Intrinsic high-sensitivity sensors based on etched single-mode polymer optical fibers," *IEEE Photonics Technol. Lett.* **27**(6), 604–607 (2015).
59. Q. Jiang, "Hydraulic pressure sensor based on fiber Bragg grating," *Opt. Eng.* **50**(6), 064401 (2011).
60. P.-L. Ko, K.-C. Chuang, and C.-C. Ma, "A fiber Bragg grating-based thin-film sensor for measuring dynamic water pressure," *IEEE Sens. J.* **18**(18), 7383–7391 (2018).
61. S. C. Her and S. Z. Weng, "Fiber Bragg grating pressure sensor integrated with epoxy diaphragm," *Sensors* **21**(9), 3199 (2021).
62. V. S. C. S. Vaddadi et al., "Design and development of pressure sensor based on fiber Bragg Grating (FBG) for ocean applications," *Eur. Phys. J. Appl. Phys.* **90**(3), 30501 (2020).
63. M. Liang, X. Fang, and Y. Ning, "Temperature compensation fiber Bragg grating pressure sensor based on plane diaphragm," *Photonic Sens.* **8**(2), 157–167 (2018).
64. M.-F. Liang et al., "A fiber Bragg grating pressure sensor with temperature compensation based on diaphragm-cantilever structure," *Optik* **145**, 503–512 (2017).
65. J. Huang et al., "A diaphragm-type fiber Bragg grating pressure sensor with temperature compensation," *Measurement* **46**(3), 1041–1046 (2013).
66. M. Manuvinakurake et al., "Design, fabrication and testing of fiber Bragg grating based fixed guided beam pressure sensor," *Optik* **158**, 1063–1072 (2018).
67. J. D. C. Jones et al., "Fibre Bragg grating based effective soil pressure sensor for geotechnical applications," *Proc. SPIE* **7503**, 75030F (2009).
68. C. Quan et al., "Diaphragm based high sensitive FBG pressure sensor," *Proc. SPIE* **8769**, 876927 (2013).
69. V. R. Pachava et al., "A high sensitive FBG pressure sensor using thin metal diaphragm," *J. Opt.* **43**(2), 117–121 (2014).
70. H. Ahmad et al., "High sensitivity fiber Bragg grating pressure sensor using thin metal diaphragm," *IEEE Sens. J.* **9**(12), 1654–1659 (2009).
71. W. Zhang, "Fiber Bragg grating pressure sensor with ultrahigh sensitivity and reduced temperature sensitivity," *Opt. Eng.* **48**(2), 024402 (2009).

72. F. Li et al., "Fiber Bragg grating soil-pressure sensor based on dual L-shaped levers," *Opt. Eng.* **52**(1), 014403 (2013).
73. Z. A. Jia et al., "Design and investigation of the fiber Bragg grating pressure sensor based on square diaphragm and truss-beam structure," *Opt. Eng.* **58**(9), 097109 (2019).
74. D. Song et al., "High-sensitivity fiber Bragg grating pressure sensor using metal bellows," *Opt. Eng.* **48**(3), 034403 (2009).
75. W. Zhang, F. Li, and Y. Liu, "FBG pressure sensor based on the double shell cylinder with temperature compensation," *Measurement* **42**(3), 408–411 (2009).
76. B.-J. Peng et al., "Pressure sensor based on a free elastic cylinder and birefringence effect on an FBG with temperature-compensation," *Measurement* **38**(2), 176–180 (2005).
77. V. R. Pachava et al., "FBG based high sensitive pressure sensor and its low-cost interrogation system with enhanced resolution," *Photonic Sens.* **5**(4), 321–329 (2015).
78. G. Lyu et al., "Design of novel FBG-based sensor of differential pressure with magnetic transfer," *Sensors* **17**(2), 375 (2017).
79. D. H. Wang et al., "An optical fiber Bragg grating force sensor for monitoring sub-bandage pressure during compression therapy," *Opt. Express* **21**(17), 19799–19807 (2013).
80. Z. Zhang, C. Shen, and L. Li, "Temperature-independent fiber-Bragg-grating-based atmospheric pressure sensor," *Opt. Commun.* **411**, 108–113 (2018).
81. Y. Liu et al., "Simultaneous pressure and temperature measurement with polymer-coated fibre Bragg grating," *Electron. Lett.* **36**(6), 564–566 (2000).
82. H. J. Sheng et al., "A lateral pressure sensor using a fiber Bragg grating," *IEEE Photonics Technol. Lett.* **16**(4), 1146–1148 (2004).
83. F. Twisk, "Rebuttal to Ickmans et al. association between cognitive performance, physical fitness, and physical activity level in women with chronic fatigue syndrome," *J. Rehabil. Res. Dev.* **50**(6), 795–810 (2013). J Rehabil Res Dev, 2013. 50(9): p. vii-viii.
84. A. Leal-Junior, A. Frizera, and C. Marques, "A fiber Bragg gratings pair embedded in a polyurethane diaphragm: towards a temperature-insensitive pressure sensor," *Opt. Laser Technol.* **131**, 106440 (2020).
85. H. J. Sheng et al., "High-sensitivity temperature-independent differential pressure sensor using fiber Bragg gratings," *Opt. Express* **16**(20), 16013–16018 (2008).
86. L. Liu et al., "Membrane-based fiber Bragg grating pressure sensor with high sensitivity," *Microw. Opt. Technol. Lett.* **51**(5), 1279–1281 (2009).
87. D. J. Hill and G. A. Cranch, "Gain in hydrostatic pressure sensitivity of coated fibre Bragg grating," *Electron. Lett.* **35**(15), 1268–1268 (1999).
88. W. T. Zhang et al., "Fiber Bragg grating pressure sensor with enhanced sensitivity," *Chin. Opt. Lett.* **5**, 507–508 (2007).
89. H.-S. Huang and T.-C. Liang, "The fabrication and analysis of lateral pressure fiber sensor based on fiber Bragg grating," *Microw. Opt. Technol. Lett.* **50**(10), 2535–2537 (2008).
90. A. Sun, "Study of simultaneous measurement of temperature and pressure using double fiber Bragg gratings with polymer package," *Opt. Eng.* **44**(3), 034402 (2005).
91. H. Ahmad et al., "High-sensitivity pressure sensor using a polymer-embedded FBG," *Microw. Opt. Technol. Lett.* **50**(1), 60–61 (2008).
92. B. K. A. Ngoi et al., "Enhanced lateral pressure tuning of fiber Bragg gratings by polymer packaging," *Opt. Commun.* **242**(4–6), 425–430 (2004).
93. L. P. Zhao, "Novel configuration for lateral pressure tuning of a fiber Bragg grating without peak splitting," *Opt. Eng.* **43**(10), 2208–2209 (2004)
94. B. Mu et al., "Fiber Bragg grating-based oil-film pressure measurement in journal bearings," *IEEE Trans. Instrum. Meas.* **68**(5), 1575–1581 (2019).
95. S. Zheng et al., "Simultaneous measurement of pressure and temperature using a single fiber Bragg grating," in *Progr. in Electromagn. Res. Symp.*, Hangzhou, China, pp. 420–423 (2005).
96. Y.-Q. Liu et al., "Fiber grating sensor with enhanced pressure and temperature sensitivity," *Chin. Phys. Lett.* **17**(2), 115–116 (2000).
97. L. Chia-Min et al., "High-sensitivity simultaneous pressure and temperature sensor using a superstructure fiber grating," *IEEE Sens. J.* **6**(3), 691–696 (2006).

98. C. -W. Lai et al., "Application of Fabry–Pérot and fiber Bragg grating pressure sensors to simultaneous measurement of liquid level and specific gravity," *Measurement* **45**(3), 469–473 (2012).
99. C. R. Dennison and P. M. Wild, "Enhanced sensitivity of an in-fibre Bragg grating pressure sensor achieved through fibre diameter reduction," *Meas. Sci. Technol.* **19**(12), 125301 (2008).
100. C. R. Dennison et al., "Validation of a novel minimally invasive intervertebral disc pressure sensor utilizing in-fiber Bragg gratings in a porcine model: an ex vivo study," *Spine* **33**(17), E589–E594 (2008).
101. Z. Liu et al., "Multifunctional smart optical fibers: materials, fabrication, and sensing applications," *Photonics* **6**(2), 48 (2019).

Siyi Xu is now pursuing her MS degree in textile science and engineering at Tianjin University of Technology. Her primary research focus is on flexible fiber Bragg grating sensors.

Xiaozhi Li joined the Institute of Smart Wearable Electronic Textiles at Tianjin University of Technology after receiving his PhD in apparel design and engineering from the same university in 2011. His research focuses on smart clothing based on flexible fiber Bragg grating sensors.

Tanyu Wang graduated her MS degree in textile science and engineering from Tianjin University of Technology in 2021. She is presently pursuing toward her PhD in textile science and engineering at the same university. She focuses her research mostly on flexible smart sensors.

Xiujuan Wang received her PhD in textile science and engineering from Tianjin University of Technology in 2022. After that, she joined working as a researcher at the Aviation Key Laboratory of Science and Technology on Life-Support Technology.

Hao Liu received his PhD in 2011 from Tianjin Polytechnic University. He is currently a professor at the School of Textile Science and Engineering of Tianjin Polytechnic University as well as the deputy director of the Institute of Smart Wearable E-Textiles. He has more than 10 years of experience in the field of flexible smart fabrics.